DESIGN AND FABRICATION OF LOW-PROFILE LOW COST 3D PRINTED RISLEY PRISM IN THE X-BAND

Nicholas Koh[1], Chia Tse Tong[2], Tay Chai Yan[2]

[1]Raffles Institution, One Raffles Institution Lane, Singapore 575954

[2]DSO National Laboratories, 12 Science Park Drive, Singapore 118225

Abstract

This paper presents the design, fabrication, optimisation, and performance of a 3D printed Risley prism. Mechanical beam steering using two transmit arrays (TAs) with independent axial rotation movements—the Risley prism approach—is chosen for its significant cost advantages over electronic beam steering. Phase wrapping is introduced in the Risley prism, successfully reducing its profile by at least 50% as compared to conventional Risley prism. The Risley prism is designed to deflect beams up to 20°. Measurement results relating to the expected beam direction agree with theory. To minimise the side-lobe levels and reduce loss from reflection, an anti-reflective coating (ARC) is implemented. With the ARC, an increase in power in the main lobe of up to 6.7dB, or 14%, was measured.

1. Introduction

Beam steering, a technique for changing the main lobe of a radiation pattern, is essential in military applications such as missile and target tracking, or object detection. In satellite communications, beam steering is also instrumental in directing EM waves towards desired devices. In such applications, beam steering technologies are selected mainly by factors such as cost, space constraints, and the speed of the beam steer. [1]

There are several approaches to beam steering, but they can be classified into 2 broad categories – electronic and mechanical beam steering. In recent years, development in technology has given rise to electronically controlled beam steering such as in phased arrays. They provide the advantage of high-speed beam steering, and extremely sleek profiles. Even though many active phased array antennas have been developed, they face large drawbacks in their high cost, energy inefficiency, and thermal management issues. Leaky wave antennas have also been proposed but they rely on frequency dependent beam steering, limiting their application in scenarios that require a fixed frequency.

The second approach harnesses mechanical beam steering. This can be achieved through feed displacement methods [2] (i.e. physically rotating the transmit or receive antenna), or through the use of phase shifting lenses such as the Luneburg lens. Even though there is no need for complicated designs, these methods face the problem of being bulky, especially when the entire antenna has to be shifted. Beam steering exploiting the Luneburg lens [3], which do not need transmit or receive modules, are also limited in their application due to the spherical shape of the Luneburg lens limiting its application in space-constrained scenarios.

This has resulted in Risley prisms gaining popularity due to their simplicity, low-cost, and good beam scanning performance. In this paper, a beam steering system exploiting the Risley prism concept is proposed, consisting of a pair of dielectric wedges that have been optimised to be at least 2 times thinner than the typical dielectric wedge with phase wrapping. They are designed to operate in the X-band at 11GHz, with a maximum scan angle of 20°. The proposed Risley prism is also optimised through an Anti-reflection coating (ARC), which was measured to improve the performance of the Risley prism by up to 14%.

2. Risley Prism Design

The conventional design of a Risley prism consists of a pair of dielectric wedges that are capable of independent axial rotation as seen in Figure 1 [4]. By varying the relative rotation angles, α_1 and α_2, of each dielectric wedge, a beam exiting the prism due to an incident plane wave can be steered in both azimuth (from 0° to 360°) and elevation (up to a limit depending on wedge properties).

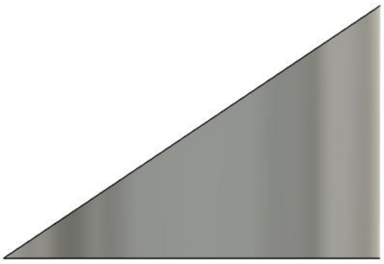

(a)

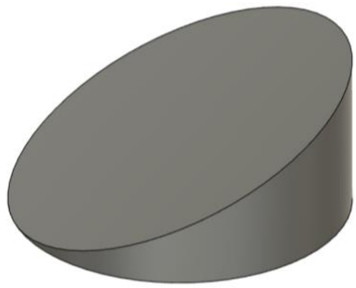

(b)

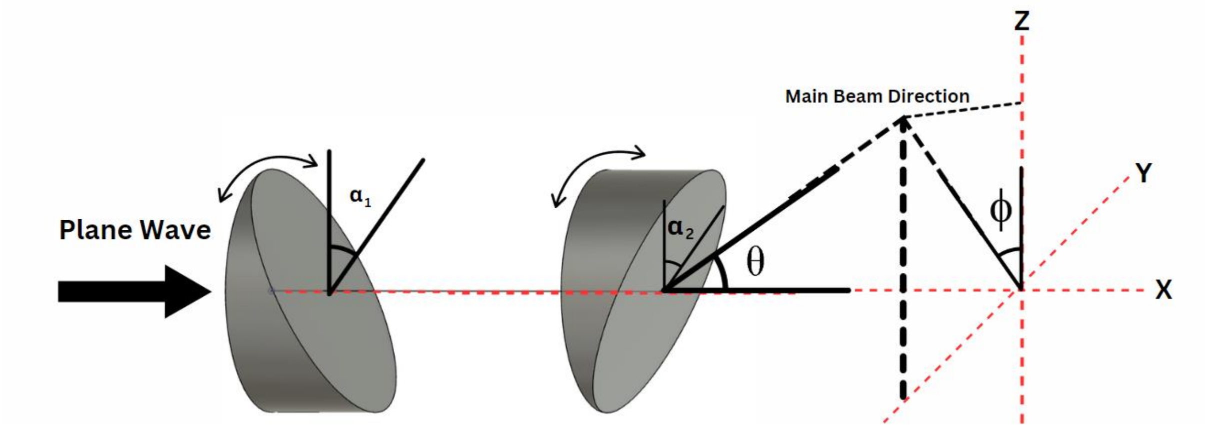

(c)

Figure 1: (a) Cross-sectional view of single wedge, (b) Perspective view of single wedge, (c) Set-up of wedges in a Risley prism.

When a plane wave passes through a dielectric wedge, refraction occurs at the slant face of the wedge due to the difference in the relative permittivities of air and the wedge. The thicker the dielectric wedge, the greater the extent of phase shift induced on the incident wave. This results in the beam deflecting toward the thicker side of the wedge which undergoes the highest extent of phase shift. While a single wedge enables deflection alongside one axis, using two wedges allows full 3D beam steering, making the dual-wedge configuration essential for versatile beam control.

An issue with current dielectric wedges is that they are bulky, heavy, and wasteful in materials. In recent years, developments in the industry have enable d the use of Printed Circuit Board (PCB) technology to develop surfaces of varying phase shift capabilities, allowing one to design a flat lens that is low profile. To achieve beam steering, developments in technology have also given rise to electronically controlled beam steering surfaces. However, all these technologies are more complicated to design.

Therefore, we propose a Risley prism that incorporates a design that hinges on phase wrapping to have the best possible outcome – lower profile and less material waste compared to conventional dielectric wedges. In Figure 2, a cross-sectional view of the design of the reduced-profile wedge of a Risley prism is shown. By harnessing phase wrapping, the bulky profile of a typical dielectric wedge can be reduced by at least 50%, with a corresponding saving in space and cost.

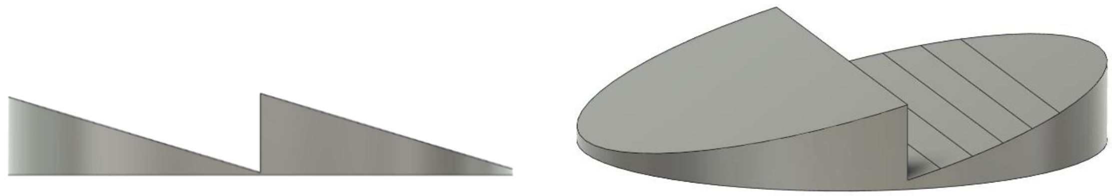

(a) (b)

Figure 2: Single wedge of a reduced-profile Risley prism (a) cross-sectional view, (b) perspective view

The material chosen for the 3-D printing of the proposed Risley prism is Polylactic Acid (PLA) due to its low cost and high accessibility to regular consumers. Before the lens was designed, the dielectric properties of PLA were measured. It was found to be 2.65 with a loss tangent of 0.00755.

The initial design of the Risley prism incorporated the idea of having different zones in a lens that each induced a phase shift of 45°, as seen in Figure 3. The mathematical equation for calculating the phase gradient of the Risley prism is given as

$$\Delta\varphi = \frac{2\pi}{\lambda} d \sin\theta \quad (1)$$

where θ is the desired beam tilt per lens, d is the width of each block of the wedge, λ is the wavelength at the desired frequency of 11 GHz, and $\Delta\varphi$ is the phase shift. The equation can then be manipulated to

$$d = \frac{\Delta\varphi \cdot \lambda}{2\pi \cdot \sin\theta} \quad (2)$$

so that the size for every 45° increment of phase shift, $\Delta\varphi$, from 0° to 360° can be calculated. After this is calculated, the height of the blocks in the wedge required to induce the respective phase shift can be calculated with equation (3) below,

$$s = \frac{\lambda}{P\left(\sqrt{\varepsilon} - 1\right)} \quad (3)$$

where s is the step height as shown in Figure 3, P corresponds to the number of corrections within a wavelength (P = 8 for a 45° phase shift), and ε is the relative permittivity of the material of the lens. Appendix 1 gives the code that was used to generate the dimensions of the Risley prism. The Risley prism was then designed on the Computer Aided Design software Fusion 360.

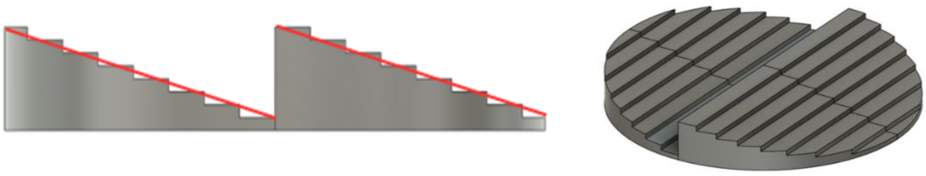

(a) (b)

Figure 3: Stepped wedge (a) cross-sectional view, (b) perspective view.

3. Theoretical Beam Direction

The limit in the angle θ, as shown in Figure 4, to which each Risley prism can steer the beam is fixed by the design of the Risley prism, when calculating the dimensions of the Risley prism in (1). The phase method was used in calculating the relative axial positions the two Risley prisms should be aligned to, α_1 and α_2, with respect to the desired beam direction, θ and ϕ. The mathematical equation for calculating the relative axial positions the Risley prisms should be aligned to, α_1 and α_2, is given by [5]

$$\alpha_1 = \phi + \frac{1}{2}\cos^{-1}[\frac{(k \sin\theta)^2}{2p^2} - 1] \quad (4)$$

$$\alpha_2 = \phi - \frac{1}{2}\cos^{-1}[\frac{(k \sin\theta)^2}{2p^2} - 1] \quad (5)$$

where p is the phase delay gradient of the Risley prism. (4) and (5) are code in Python (see Appendix 3) to predict the beam steer angle. A plot as seen in Figure 5 was then created on MATLAB to show how θ varies with α_1 and α_2. The code can be found in Appendix 4.

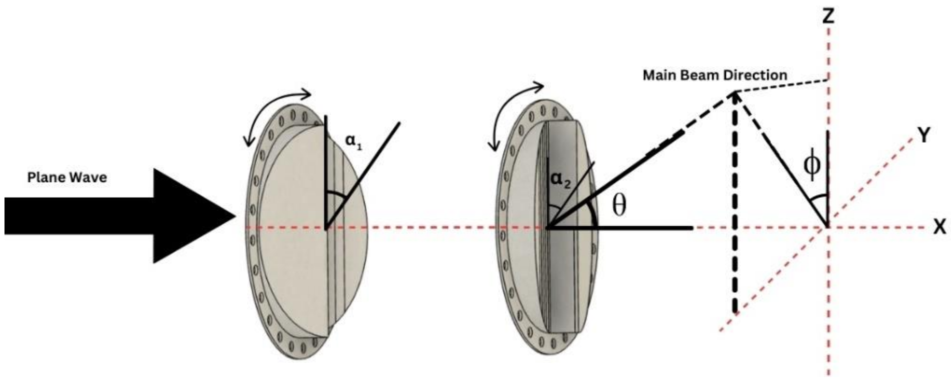

Figure 4: Angles in Risley prism for beam direction derivation.

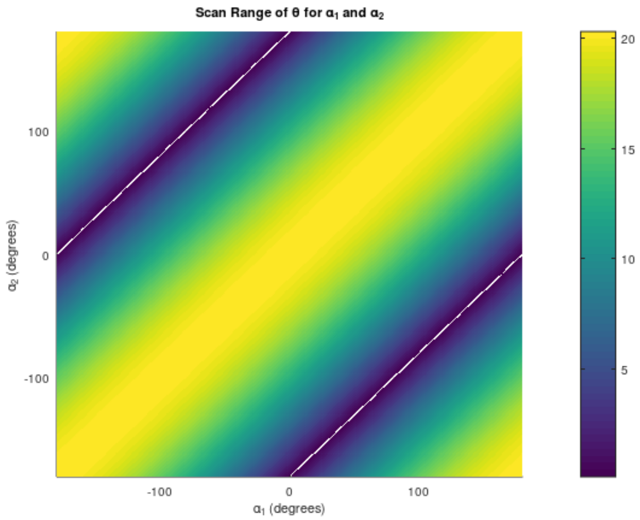

Figure 5: Theoretical beam direction as a function of α_1 and α_2.

4. Anti-Reflection Coating

Anti-reflection coating is a thin layer of dielectric material, with a specially chosen thickness, added to a dielectric layer to reduce the reflection between the dielectric and air interface. To reduce the energy losses due to reflection from the flat face of the first Risley prism wedge (where a plane wave will impinge normally on it), an ARC is added to the flat side of both wedges.

The optimal permittivity of the ARC, ε_{ARC}, is given by [6]

$$\varepsilon_{ARC} = \sqrt{\varepsilon_0 \varepsilon_1} \tag{6}$$

where ε_0 is the relative permittivity of the surrounding material (which in this case is air) and ε_1 is the relative permittivity of the dielectric of the Risley prism. The thickness of the ARC, t_{ARC}, is chosen to be

$$t_{ARC} = \frac{\lambda}{4\varepsilon_{ARC}} \tag{7}$$

Apart from the relative permittivity, another factor that affects its optimum value is the height of the Risley prism above the ARC. The relative permittivity of the ARC can be varied by adjusting the internal volume of the ARC layer. This could be done by placing equally spaced apart square holes of side, *B*, in the ARC (as shown in Figure 6) to reduce the volume of the ARC layer and by doing so, the relative permittivity of the ARC is reduced.

Unit cell simulation in CST Studio Suite [7] was done to find the lowest reflection coefficient (S11) and highest transmission coefficient (S21) when varying the hole size, *B*. This was calculated for every step height, *C*. Figure 6 shows the simulation set-up in CST Studio Suite. A unit cell of size 10mm was used. Table 1 shows the optimised hole size at every height of the Risley prism above it.

Figure 7 shows the optimised ARC layer. As the thickness of the ARC is less than a quarter wavelength, the effect of the phase shift induced by the ARC was assumed to be negligible in affecting the beam steering function of the Risley prism.

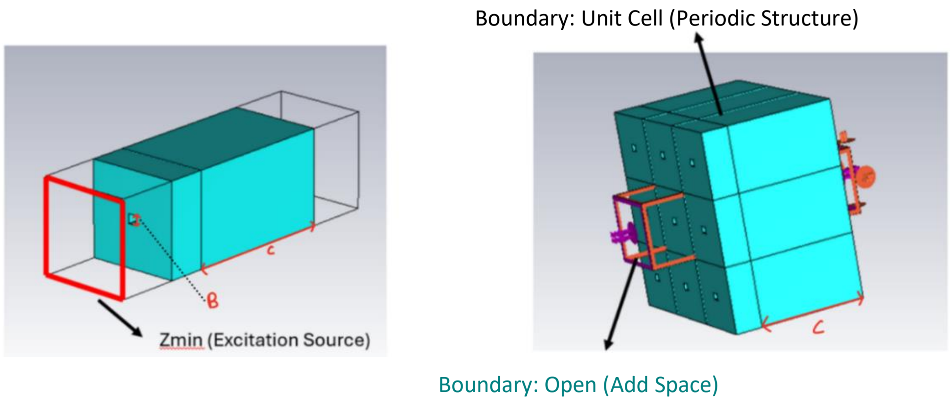

(a) (b)

Figure 6: (a) Unit Cell Simulation on CST Studio Suite, (b) Boundary Set-up on CST Studio Suite

Table 1: Optimised hole size (B) for each step height (C)

C (mm)	Optimised B (mm)	S11 (dB)	S21(dB)
9.94	10	-11.5	-0.465
12.533	1	-39.5	-0.229
15.126	8	-16.8	-0.320
17.719	10	-15.2	-0.382
20.312	0	-19.0	-0.387
22.905	7	-16.8	-0.438
25.498	10	-22.8	-0.374
28.091	0	-13.7	-0.626
30.684	6	-18.3	-0.525
33.277	10	-27.1	-0.462
35.870	5.5	-11.0	-0.880
38.463	5	-22.4	-0.595
41.056	9	-22.0	-0.593
43.649	9	-11.3	-0.942
46.242	3	-44.5	-0.682

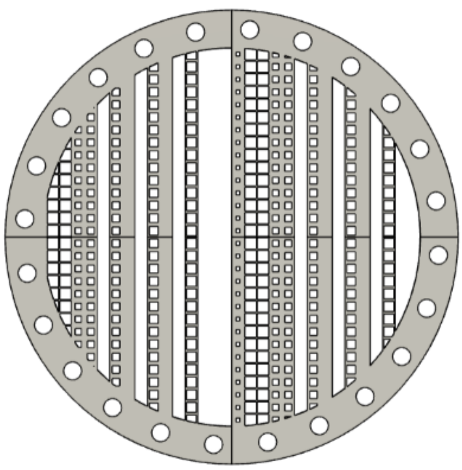

Figure 7: ARC.

5. Measurement Results

The Risley prisms were fabricated using the 3D printer Ender-3 V3 SE, with a nozzle size of 0.4mm. The Risley Prisms were then measured in a bistatic chamber at TL@NUS as shown in Figure 8. The transmit antenna is on the right while the receive antenna which was connected to a Vector Network Analyser (VNA) is on the left. The VNA measured the receive power. 2 half-lenses, on the transmit antenna and receive antenna, were used to focus the electromagnetic radiation onto the antennas, and to ensure the beam approaching the Risley prism was collimated.

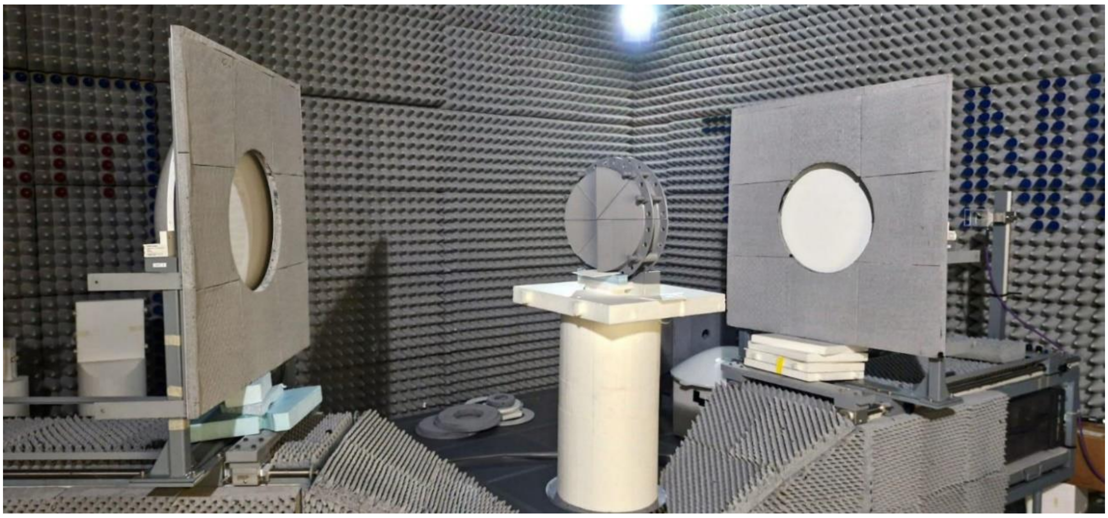

Figure 8: Measurement set-up.

As the measurement results heavily involved the ability of the Risley prism to steer the beam, limiting the power of electromagnetic radiation that did not pass through the lens was important to prevent an errantly high gain from being detected at 0°, or directly in front of the lens. Therefore, two large absorber screens added to reduce the spillover and improve the accuracy of the results. 4 configurations of the Risley Prism, as detailed in Figure 10, were measured. The same configuration was then repeated with the ARCs. The received power pattern was measured along the XY plane as seen in Figure 10, from -30° to 30°, with the positive X axis being 0°. The right arm and the Risley prism were fixed while the left arm of the measurement system was manually rotated and readings taken at 1° interval to obtain the received power pattern, as seen in Figure 9.

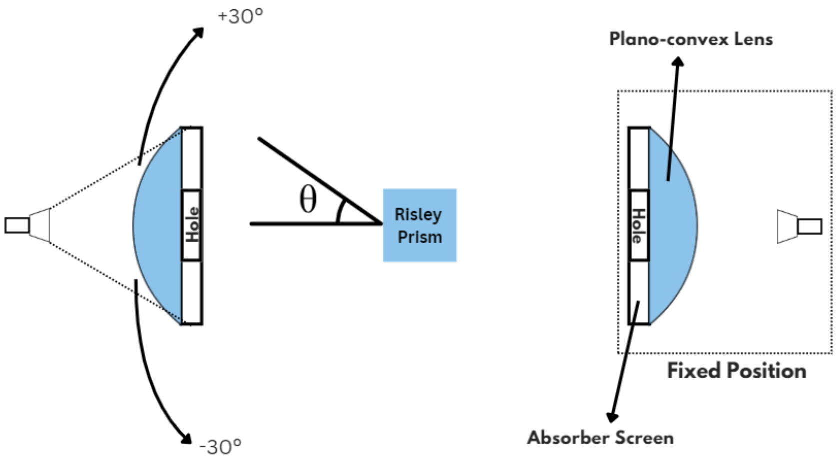

Figure 9: Measurement Set-up Diagram

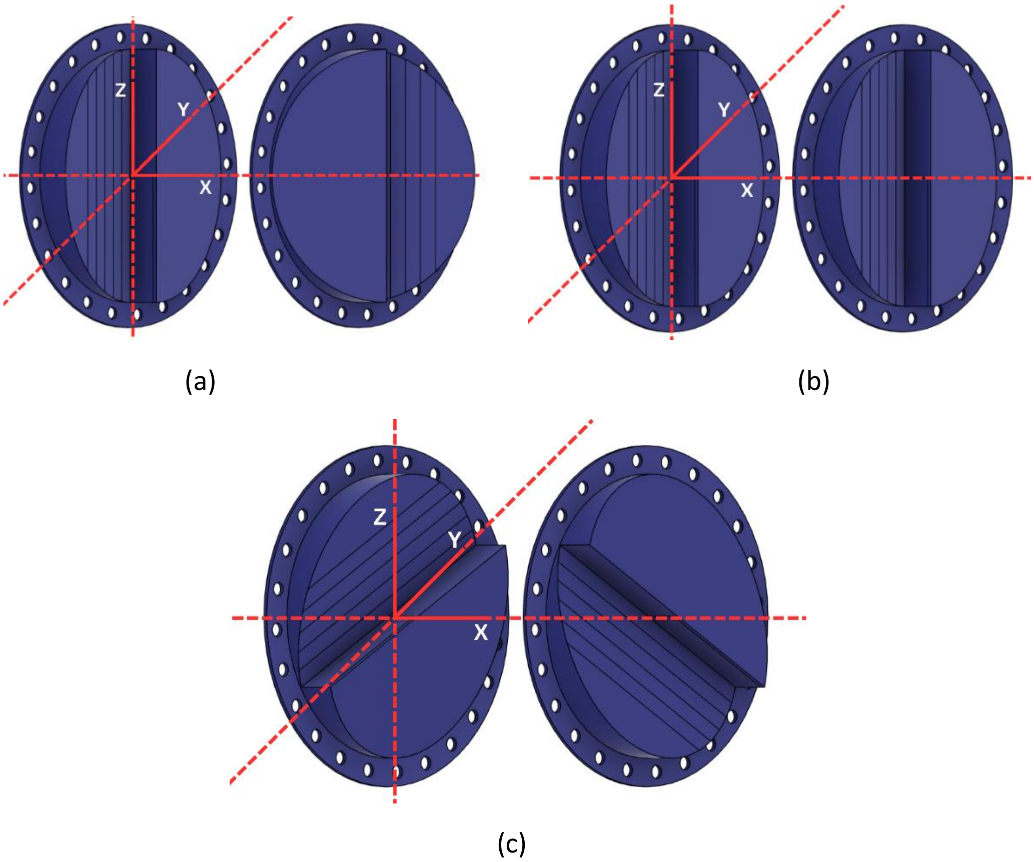

Figure 10: Relative orientation of wedges of Risley prism. (a) α_1 = 0°, α_2 = 180°, (b) α_1 = -90°, α_2 = 90°, (c) α_1 = -60°, α_2 = 60°

Figure 11 shows the full measurement results, comparing the measured power with and without the ARC. As summarised in Table 2, the measured beam direction, θ, is in close agreement with the theoretical beam direction. Minor differences between theory and measurement can be attributed to alignment accuracy in the actual set up that were difficult to avoid. The effect of the Risley prism can be seen in how the main beam shifts away from 0° when no Risley prism is used.

Significant gains in power were observed with all implementations of the ARC, especially in the configurations where α_1, α_2 values were (-60°, 60°). The increase is 6.7dB for this case, or 24.6%.

Table 2: Simulation and Measurement Results

			Without ARC		With ARC	
α_1/°	α_2/°	Expected θ/°	Measured θ/°	Measured Power/dB	Measured θ/°	Measured power/dB
0	180	0	3	-39.6	-1	-38.8
-90	90	19.9	20	-43.4	20	-43.2
-60	60	17.5	16	-47.9	15	-41.2

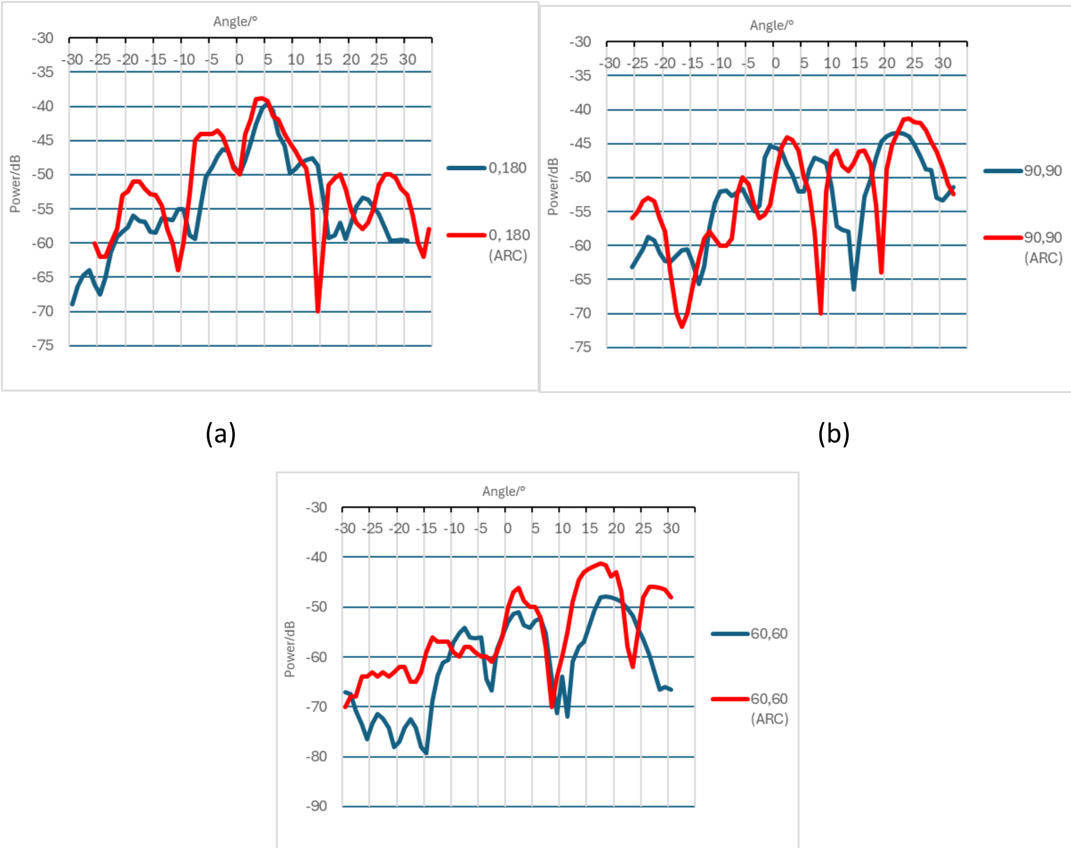

(a) (b)

(c)

Figure 11: Measurement Results (a) α_1 = 0°, α_2 = 180°, (b) α_1 = -90°, α_2 = 90°, (c) α_1 = -60°, α_2 = 60°

6. Further Work

Due to technological constraints in the 3D printer used in our project, warping, the phenomenon of material shrinkage during the printing process, occurred. During the process of the 3D print, the bed is heated to 70°C and plastic is extruded from the nozzle at 225°C (this varies from material to material). Due to the relative thickness of our print, as well as how we were printing the model at 100% infill, during the print, the model would unavoidably contract due to internal stresses arising from the uneven temperature throughout the model. Even though preventive measures were taken such as printing a brim to increase the adhesion of the first layer to the bed, and reducing the cooling fan speed on the model, the effect of the warp could only be minimised but not fully eliminated. Figure 12 shows the effect of the warp on the Risley prism. It is concluded that a 3D printer equipped with a heated enclosure is required, so that the temperature surrounding the model is high as well to reduce the unevenness of heat distribution throughout the model.

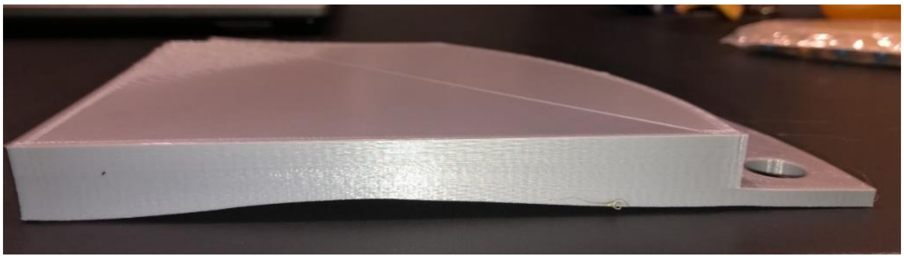

Figure 12: Warp on Risley prism.

In addition, to further reduce losses from reflection and hence increase transmission efficiency, the ARC presented could be added on both the flat side and the sloped side of the Risley prism. In this paper, due to the relatively thin thickness of the ARC of about a quarter wavelength, the phase shifting capabilities of the ARC were considered as negligible. However, in applications where an extremely precise beam steer is required, this effect cannot be ignored, as adding additional phase shift at different zones of the Risley prism already designed to have a specific phase shift would disrupt the direction of the beam. Hence, different designs of the ARC such as an ARC with a uniform pattern could be implemented.

Due to phase wrapping in this reduced-profile Risley prism, the bandwidth of the Risley prism is now limited as compared to the conventional Risley prism, where because there is no phase wrap, the Risley prism is able to achieve wideband beam scanning. Hence, other techniques that are able to reduce the profile of the Risley prism while ensuring that its wideband properties are not disrupted such as a Phase-Shifting Surfaces (PSS) exploiting Printed Circuit Board (PCB) technology could be explored.

7. Conclusion

In this paper, a low-profile, low-cost 3D printed Risley prism at 11GHz is presented. It harnessed phase wrapping to reduce the profile of a regular dielectric wedge prism by more than half, and achieved a maximum scanning angle of 20°. Furthermore, the main lobe direction at the 4 configurations used in the paper agree with the theoretical beam direction. The Risley prism managed to achieve its key purpose – beam scanning, and with the ARC, its performance has been improved by up to 14%. The use of 3D printing technology in manufacturing the Risley prism also demonstrated the useful application of this technology where customisability and speed is important. I believe that this design can contribute to many beam scanning applications, especially when cost, ease of design and manufacturability, and space need to be prioritised.

ACKNOWLEDGEMENT

I would like to sincerely thank my mentors, Dr Chia Tse Tong and Dr Tay Chai Yan, for their patience in teaching me abstract concepts. They have taken time throughout the year to not only provide insights into the project from their years of experience, but also to nurture in me meaningful skills and values that I have picked up over the research process. I would also like to thank DSO National Laboratories for giving me the rare and irreplaceable opportunity to embark on this project. In addition, I am also grateful to Temasek Laboratories (TL@NUS) for allowing me to use their measurement facilities.

REFERENCES

[1] García-Torales, G. (2022). Risley Prisms Applications: An overview. Advances in 3OM: Opto-Mechatronics, Opto-Mechanics, and Optical Metrology, 48. https://doi.org/10.1117/12.2616071

[2] Nayeri, P., Yang, F., Elsherbeni, A.Z.: ‘Bifocal design and aperture phase optimizations of reflectarray antennas for wide-angle beam scanning performance’, IEEE Trans. Antennas Propag., 2013, 61, (9), pp. 4588–4597

[3] Marin, J.G., Hesselbarth, J.: ‘Lens antenna with planar focal surface for wide-angle beam-steering application’, IEEE Trans. Antennas Propag., 2019, 67, (4), pp. 2757–2762

[4] Zhang, Z., Luyen, H., Booske, J. H., & Behdad, N. (2020). X ‐ band, mechanically ‐ beam ‐ steerable lens antenna exploiting the Risley Prism Concept. IET Microwaves, Antennas & Propagation, 14(14), 1902‐1908. https://doi.org/10.1049/iet-map.2020.0249
[5] Wang, J., & Ramhat-Samii, Y. (2019). Phase method: A more precise beam steering model for phase-delay metasurface based Risley Antenna. 2019 URSI International Symposium on Electromagnetic Theory (EMTS), 1–4. https://doi.org/10.23919/ursi-emts.2019.8931513
[6] Tan, X., Zhai, H., Meng, K., & Zhang, Z. (2021). Anti-reflection for monocrystalline silicon from diamond-like carbon films deposited by Magnetron Sputtering. Materials Research Express, 8(9), 096402. https://doi.org/10.1088/2053-1591/ac2445.
[7] CST Studio Suite 2024 version.

Appendix 1 (Risley Prism Specifications Generator):

```python
import numpy as np
import math
theta = np.radians(10)  # Desired beam tilt per lens
lamda = 0.0272538598 * 1000  # Wavelength at 11 GHz
phi = 0  # Phase shift
d = 0  # Initial value of d


# Loop to calculate d until d exceeds 150 which is the radius of the lens
while d < 150:
    d = (phi * lamda) / (2 * np.pi * np.sin(theta))
    phi += 0.785398
    print(d) # Calculates the distance from the centre of the lens at which the respective phi (phase shift) occurs


print("Step Height Calculation")
e = 2.65
s = lamda/(8*(math.sqrt(e)-1)) #step height
p = 1
while p<9: #Generates the 8 step heights
    print(s*p)
    p = p + 1
```

Appendix 2 (Risley Prism Configuration Calculator)

```
import numpy as np
import math

theta = 10 #Desired beam direction
phi = 10 #Desired beam direction

wavelength = 0.02725385981818
desired_theta = math.radians(theta) #radian
desired_phi = math.radians(phi) #radian
k = (2 * np.pi) / wavelength
p_sq = ((2*np.pi)/0.156949)**2 #change in phase /  distance


alpha_1 = desired_phi + (0.5 * np.arccos( ( (k*np.sin(desired_theta))**2 /
    (2*p_sq) ) - 1))

alpha_2 = desired_phi - (0.5 * np.arccos( ( (k*np.sin(desired_theta))**2 /
    (2*p_sq) ) - 1))

print(math.degrees(alpha_1))
print(math.degrees(alpha_2))
```

Appendix 3 (Theoretical Beam Direction Calculator):

```
import numpy as np
import math

theta = 0
phi = 0

wavelength = 0.02725385981818
desired_theta = math.radians(theta) #radian
desired_phi = math.radians(phi) #radian
k = (2 * np.pi) / wavelength
p_sq = ((2*np.pi)/0.156949)**2 #change in phase /  distance


alpha_1 = desired_phi + (0.5 * np.arccos( ( (k*np.sin(desired_theta))**2 / (2*p_sq) ) - 1))

alpha_2 = desired_phi - (0.5 * np.arccos( ( (k*np.sin(desired_theta))**2 / (2*p_sq) ) - 1))

print(math.degrees(alpha_1))
print(math.degrees(alpha_2))
```

Appendix 4 (Theoretical Beam Direction Plot Generator on MATLAB):

```
k = 230.542952568;
p = 40.0332930263;

alpha1_range = linspace(-180, 180, 360);
alpha2_range = linspace(-180, 180, 360);

alpha1_rad = deg2rad(alpha1_range);
alpha2_rad = deg2rad(alpha2_range);
[alpha1, alpha2] = meshgrid(alpha1_rad, alpha2_rad);

cos_theta_sq = (p^2 * (cos(alpha1) + cos(alpha2)).^2 + ...
                p^2 * (sin(alpha1) + sin(alpha2)).^2) / k^2;

cos_theta_sq(cos_theta_sq > 1) = 1;
theta = rad2deg(asin(sqrt(cos_theta_sq)));
alpha1_deg = rad2deg(alpha1);
alpha2_deg = rad2deg(alpha2);

figure;
surf(alpha1_deg, alpha2_deg, theta, 'EdgeColor', 'none');
xlim([-180 180]);
ylim([-180 180]);
xlabel('\alpha_1 (degrees)');
ylabel('\alpha_2 (degrees)');
zlabel('\theta (degrees)');
title('Scan Range of \theta for \alpha_1 and \alpha_2');
colorbar;
```